Electronic Supplementary Information (ESI)

Fe-N_4 and Co-N_4 dual sites for boosting oxygen electroreduction in Zn-air batteries

Dan Wang, [a] Hao Xu, [a] Peixia Yang,* [a] Xiangyu Lu, [a] Jingyuan Ma,* [b] Ruopeng Li, [a] Lihui Xiao, [a] Jinqiu Zhang, [a] Maozhong An, [a]

[a] MIIT Key Laboratory of Critical Materials Technology for New Energy Conversion and Storage, School of Chemistry and Chemical Engineering, Harbin Institute of Technology, 150001 Harbin, China.

[b] Shanghai Synchrotron Radiation Facility, Zhangjiang Laboratory (SSRF, ZJLab), Shanghai Advanced Research Institute, Chinese Academy of Sciences, Shanghai, 201204 China

*E-mail: yangpeixia@hit.edu.cn; majy@sari.ac.cn

Characterization

The detailed morphology of materials was observed by scanning electron microscopy (SEM, Quanta 200FEG) and transmission electron microscopy (TEM, FEI Talos F200x). The structure of the samples was investigated by a Bruker D8 diffractometer X-ray diffraction (XRD). Raman spectra were recorded by a Raman spectrometer (HR800, JY Company). The Brunauer-Emmett-Teller (BET) surface area and pore size distribution were evaluated by recording nitrogen adsorption-desorption isotherms using a gas adsorption analyzer (Bei Shi De 3H-2000PS1). X-ray absorption spectra at Fe K-edge and Co K-edge were performed on the BL14W1 beam line at the Shanghai Synchrotron Radiation Facility (SSRF), Shanghai Advanced Research Institute, China[1]. The EXAFS raw data were background subtracted, normalized, Fourier transformed, and fitted by the standard procedures using the Athena and Artemis software packages[2]. X-ray photoelectron spectroscopy (XPS) were collected on a Physical Electronics PHI model 5700 instrument. Binding energy of all samples was calibrated with respect to the standard C1s binding energy (284.8 eV).

Electrochemical measurements

The polarization curve test for ORR was performed in N_2- or O_2-saturated 0.1 M KOH solution at a scan rate of 10 mV s^{-1}. The ORR polarization curves were recorded at different rotating rates ranging from 900 to 2500 rpm. The electron transfer number (n) was calculated according to the Koutecky-Levich equation:

$$\frac{1}{j} = \frac{1}{j_L} + \frac{1}{j_K} = \frac{1}{B\omega^{\frac{1}{2}}} + \frac{1}{j_K} \tag{1}$$

$$B = 0.2nFC_O D_O^{\frac{2}{3}} v^{-\frac{1}{6}} \tag{2}$$

where j is the measured current density (mA cm^{-2}), j_L and j_K are the diffusion-limited and kinetics current densities (mA cm^{-2}), respectively, ω is the rotation rate of the RDE (rpm), F is the Faraday constant (96485 C mol^{-1}), C_O is the bulk concentration of O_2 in 0.1 M KOH (1.2×10^{-6} mol cm^{-3}), D_O is the diffusion coefficient of O_2 in 0.1 M KOH and 0.1 M $HClO_4$ solution (1.9×10^{-5} cm^2 s^{-1}), and v is the kinematic viscosity of the electrolyte (0.01 cm^2 s^{-1}).

The specific kinetic current density was also calculated from the K-L equation:

$$j_K = \frac{j_L \times j}{j_L - j} \tag{3}$$

In addition, rotating ring-disk electrode (RRDE) tests were applied to evaluate the hydrogen peroxide yield (H_2O_2%) and the electron transfer number (n) based on the equations as follows:

$$H_2O_2(\%) = 200\frac{I_R/N}{I_D + I_R/N} \tag{4}$$

$$n = 4\frac{I_D}{I_D + I_R/N} \tag{5}$$

where I_D and I_R are disk and ring current, respectively, N is the collection efficiency of the Pt ring (37%).

Turnover frequency (TOF) of the Co-N-C, Fe-N-C and FeCo-N-C were calculated using the equation:

$$TOF = \frac{j \times a}{4 \times m \times F} \tag{6}$$

Where j is the measured current density at 0.9 V, a is the surface area of the RDE (0.196 cm^{-2}), 4 is the electron transfer number of ORR, m is the mole number of active Co atomic sites, Fe atomic sites, and dual atomic sites on the RDE, and F is the Faraday constant (F = 96485 C mol^{-1}).

Electrochemical impedance spectroscopy (EIS) measurements were carried out in a frequency range of 100 kHz to 0.01Hz with an AC voltage with 5 mV amplitude.

The stability of samples was evaluated by accelerated durability test (ADT). The alkaline and acidic ORR ADT was performed by applying potential cycling between 1.0 and 0.6 V *vs.* RHE at a scan rate of 50 mV s^{-1} for 5000 cycles in O_2-saturated 0.1 M KOH and 0.1 M $HClO_4$, respectively.

Computational details

The adsorption energy (E_{ads}) of the adsorbates on the studied Co-N_4, Fe-N_4, and Fe-N_4&Co-N_4 site was defined as

$$E_{ads} = E_{total} - E_{mol} - E_{sub} \quad (7)$$

where E_{total}, E_{mol}, and E_{sub} are the total energies of the molecules adsorbed on Co-N_4, Fe-N_4, and Fe-N_4&Co-N_4 site, the isolated adsorbate molecules, and adsorption substrate (Co-N_4, Fe-N_4, and Fe-N_4&Co-N_4 site), respectively[3]. The free energy of the ORR intermediates was calculated by the thermodynamic model proposed by Nørekov et al.[4].

$$\Delta G = \Delta E + \Delta ZPE + T\Delta S + \Delta G_U + \Delta G_{pH} + \Delta G_{field} \quad (8)$$

where ΔE is the reaction energy obtained from the DFT calculations, ΔZPE is the zero-point energy, ΔS is the entropy, and $\Delta GU = -neU$, where n is the electron transfer number and U is the applied potential (*vs.* RHE). In this work, ΔG_{pH} and ΔG_{field} are not involved.

Zn-air battery tests

The liquid Zn-air battery tests were performed at room temperature. The catalyst layer was prepared as follows: FeCo-N-C (2.5 mg), acetylene black (1 mg), activated carbon (4 mg), and Nafion (5 wt%, 8 μL) were dispersed in 200 μL of isopropyl alcohol followed by sonicating for 20 min to form a homogeneous catalyst ink; Ni foams as the substrate were immersed in 1 M HCl solution and then washed with ethanol and ultrapure water before use; the catalyst ink was dropped onto the Ni foam with a mass loading of 2 mg cm^{-2} and then dried in vacuum at 50 ℃ for 12 h. The commercial Pt/C (20 wt%) was used as catalyst layer for comparison with the same loading. A polished zinc foil was employed as the anode, while 6 M KOH solution was employed as the electrolyte. The polarization curves test was carried out on a CHI760E electrochemical workstation. The galvanostatic discharge test was performed in the LAND CT2001A testing system.

The all-solid-state Zn-air battery was assembled by a polished zinc foil as anode, and a piece of Ni foam coated by catalyst as cathode. The gel polymer as solid electrolyte was prepared following the procedures: 5 g polyvinyl alcohol (PVA) was added into 45 mL H_2O under vigorously stirring; and then 5 mL KOH solution (1 g mL^{-1}) was poured into the above solution and stirred for 40 min at 95 °C. Subsequently, the gel was spread in a culture dish and frozen for 6 h, and

placed at room temperature for 10 h. The zinc foil and catalyst coated Ni foam were placed on the two sides of PVA gel film wetted by 6 M KOH electrolyte. The catalyst loading of the all-solid-state Zn-air battery was the same as that of the liquid Zn-air battery.

References

1 H. S. Yu, X. J. Wei, J. Li, S. Q. Gu, S. Zhang, L. H. Wang, J. Y. Ma, L. N. Li, Q. Gao, R. Si, F. F. Sun, Y. Wang, F. Song, H. J. Xu, X. H. Yu, Y. Zou, J. Q. Wang, Z. Jiang and Y. Y. Huang, *Nuclear Science and Techniques* 2015, 26, 050102.

2 M. Newville, *Journal of Synchrotron Radiation*, 2001, 8, 322-324.

3 H. Xu, D. Wang, P. Yang, A. Liu, R. Li, Y. Li, L. Xiao, J. Zhang and M. An, *Physical Chemistry Chemical Physics*, 2020, DOI: 10.1039/D0CP04676K.

4 A. A. Peterson, F. Abild-Pedersen, F. Studt, J. Rossmeisl and J. K. Norskov, *Energy Environ. Sci.*, 2010, 3, 1311-1315.

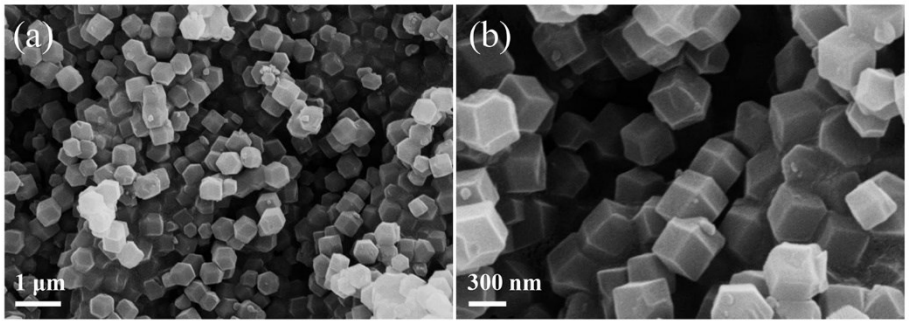

Fig. S1 SEM images of ZIF-8.

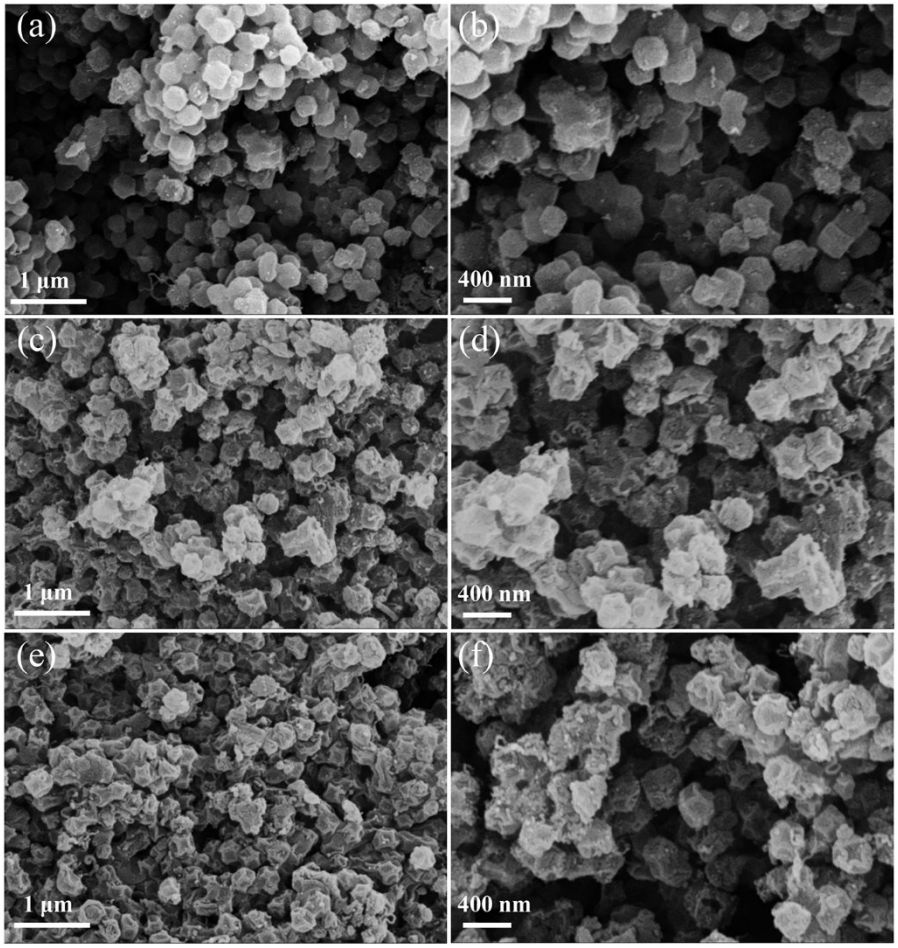

Fig. S2 SEM images of (a, b) Co-N-C, (c, d) Fe-N-C and (e, f) FeCo-N-C.

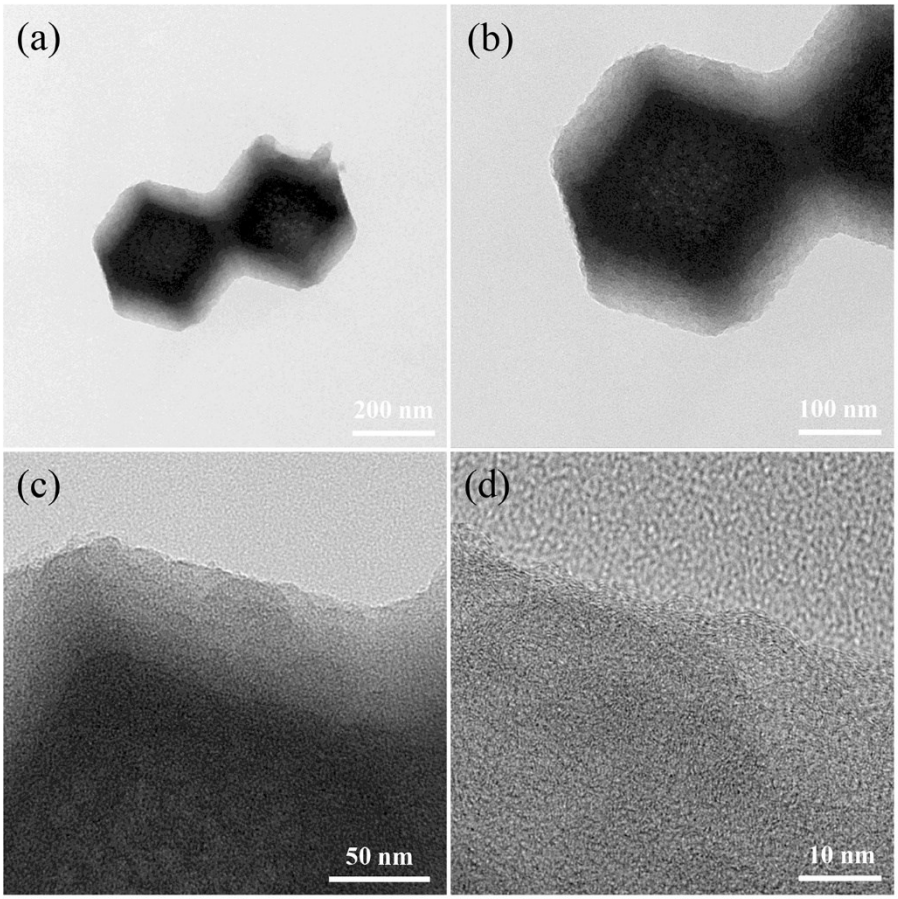

Fig. S3 (a-c) TEM and (d) HRTEM images of Co-N-C.

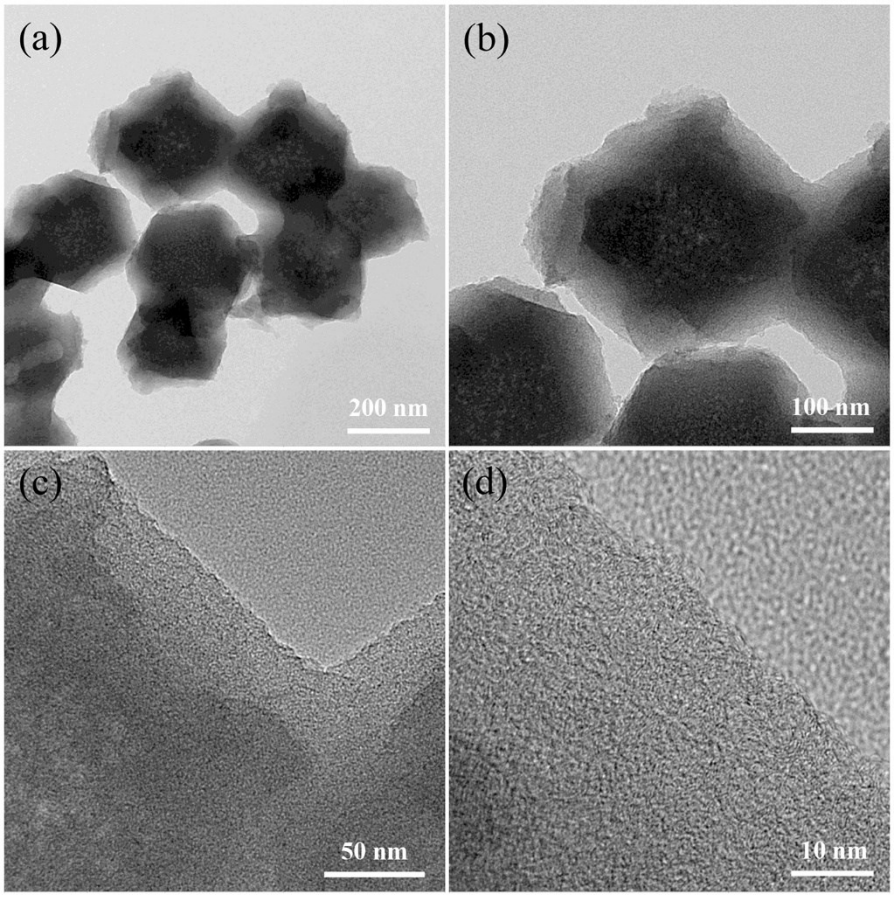

Fig. S4 (a-c) TEM and (d) HRTEM images of Fe-N-C.

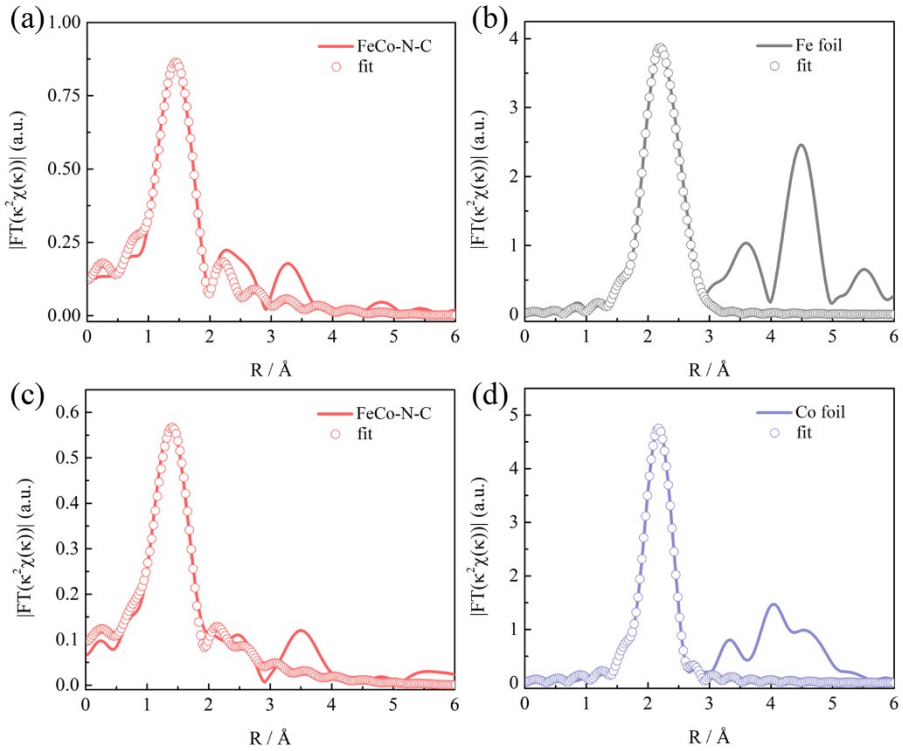

Fig. S5 Comparison between the fitting results and experimental FT-EXAFS data at Fe K-edge for (a) FeCo-N-C and (b) standard Fe foil. Comparison between the fitting results and experimental FT-EXAFS data at Co K-edge for (c) FeCo-N-C and (d) standard Co foil.

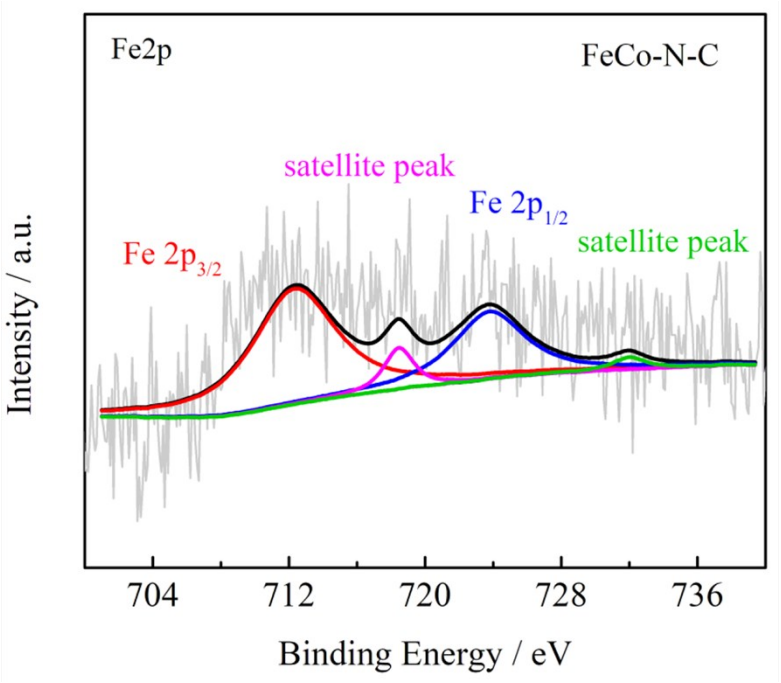

Fig. S6 High-resolution Fe 2p XPS spectrum of FeCo-N-C.

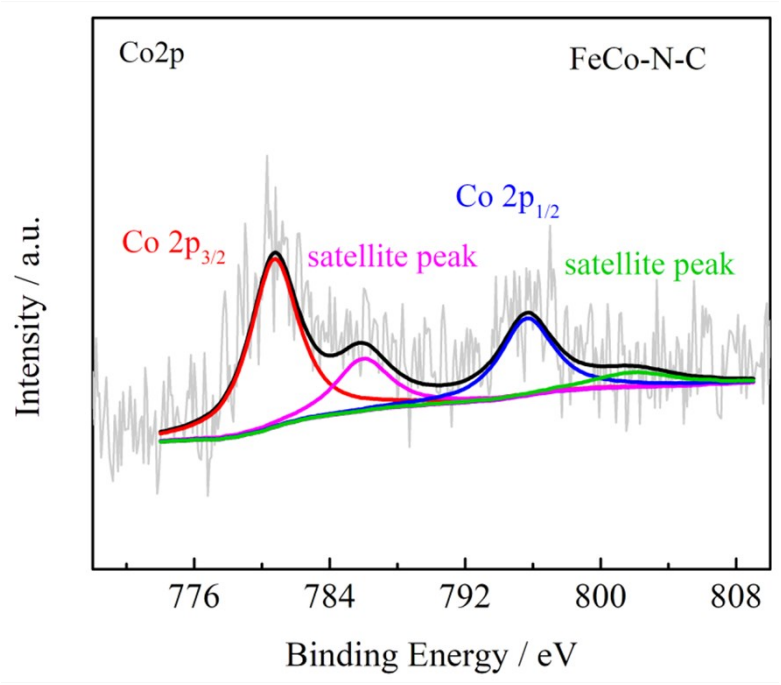

Fig. S7 High-resolution Co 2p XPS spectrum of FeCo-N-C.

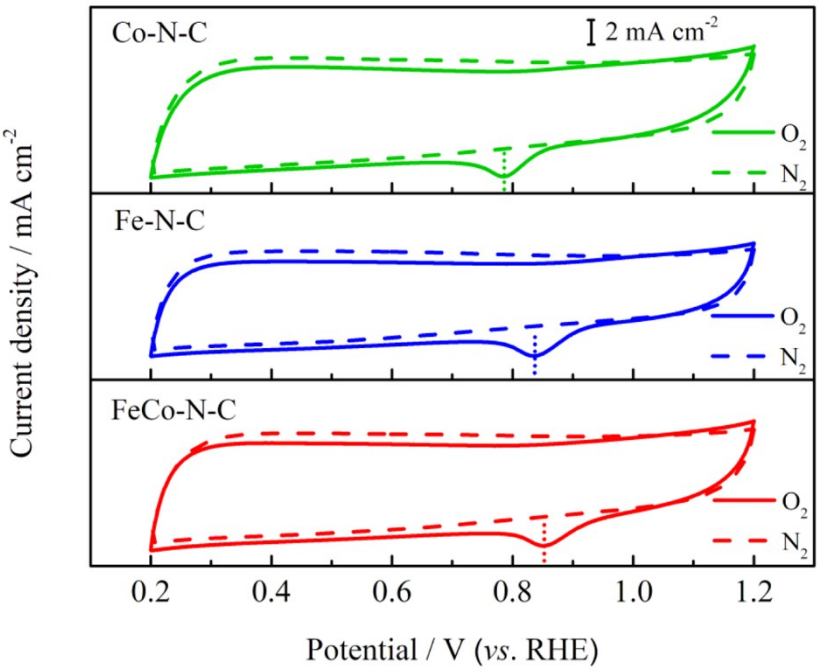

Fig. S8 CV curves for Co-N-C, Fe-N-C and FeCo-N-C catalysts at a scan rate of 50 mV s^{-1} in O_2 and N_2-satuated 0.1 M KOH, respectively.

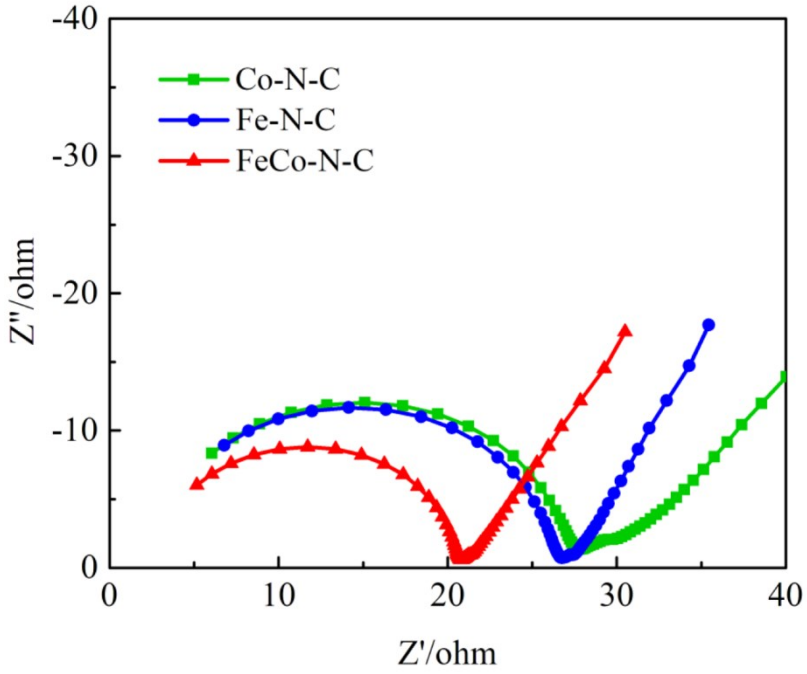

Fig. S9 The electrochemical impendence spectroscopy of Co-N-C, Fe-N-C and FeCo-N-C.

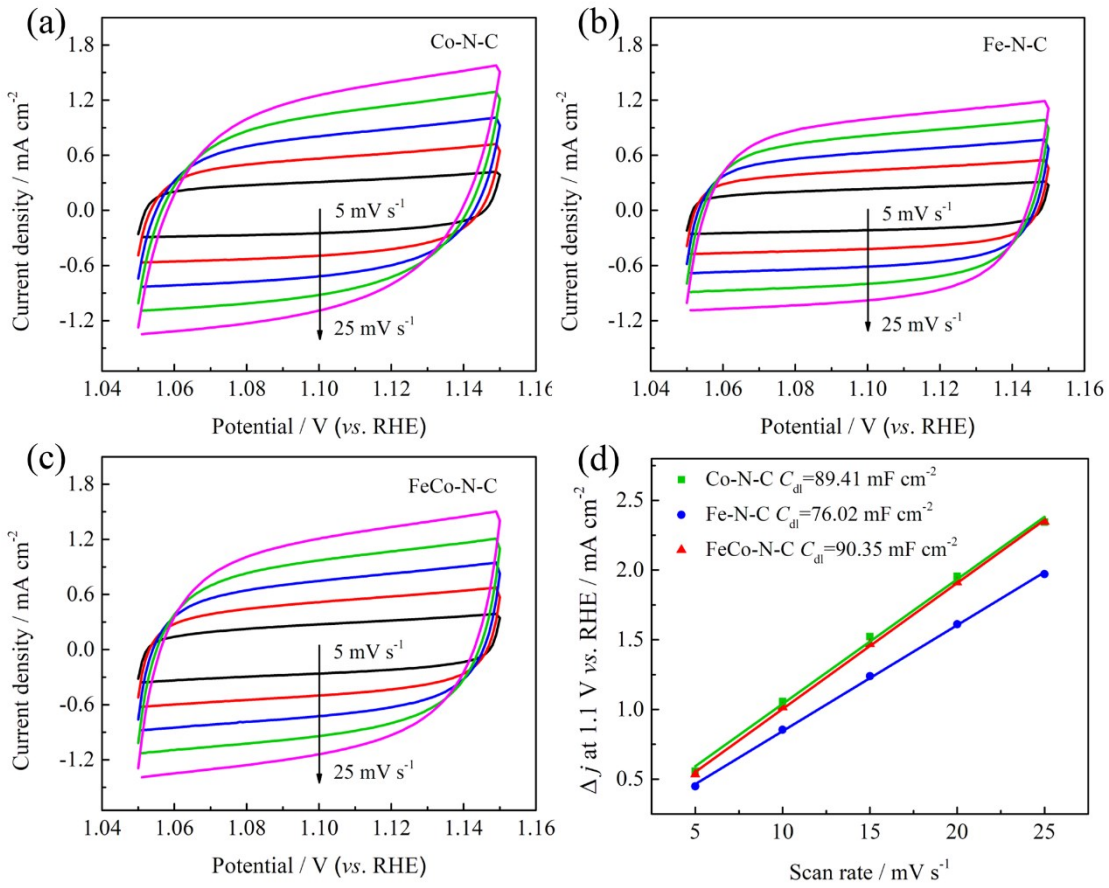

Fig. S10 CV curves for (a) Co-N-C, (b) Fe-N-C and (c) FeCo-N-C at different scan rates of 5, 10, 15, 20 and 25 mV s^{-1} in O_2-satuated 0.1 M KOH. (d) Plots of current densities (at 1.1 V *vs*. RHE) as a function of scan rates.

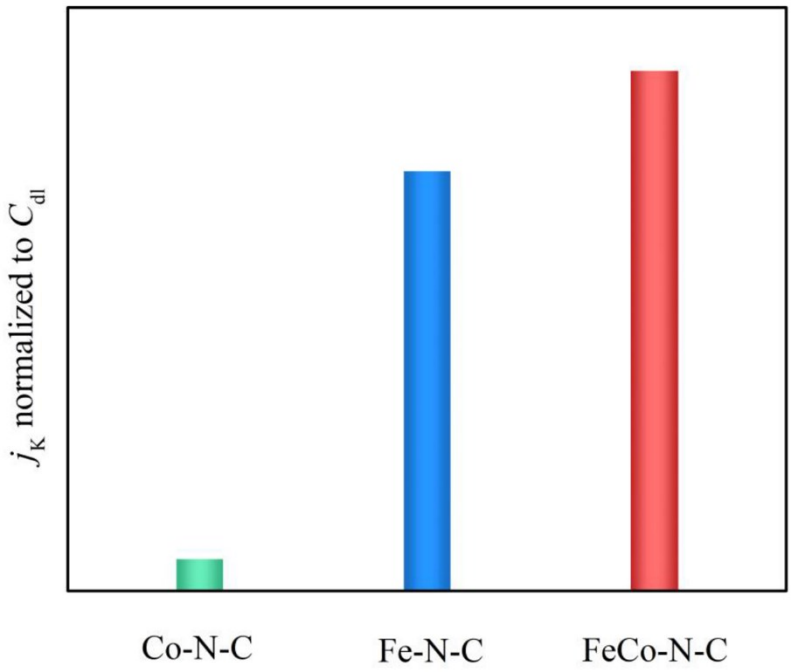

Fig. S11 The j_K@0.9 V with respect to C_{dl} for Co-N-C, Fe-N-C and FeCo-N-C.

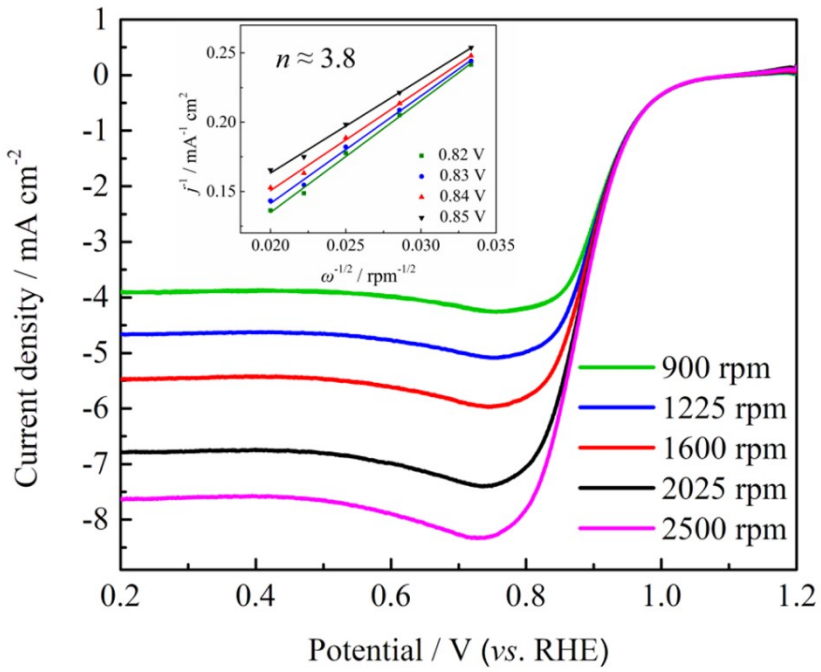

Fig. S12 ORR polarization curves at different rotating rates in 0.1 M KOH. Inset: the fitted K-L plots and electron transfer numbers.

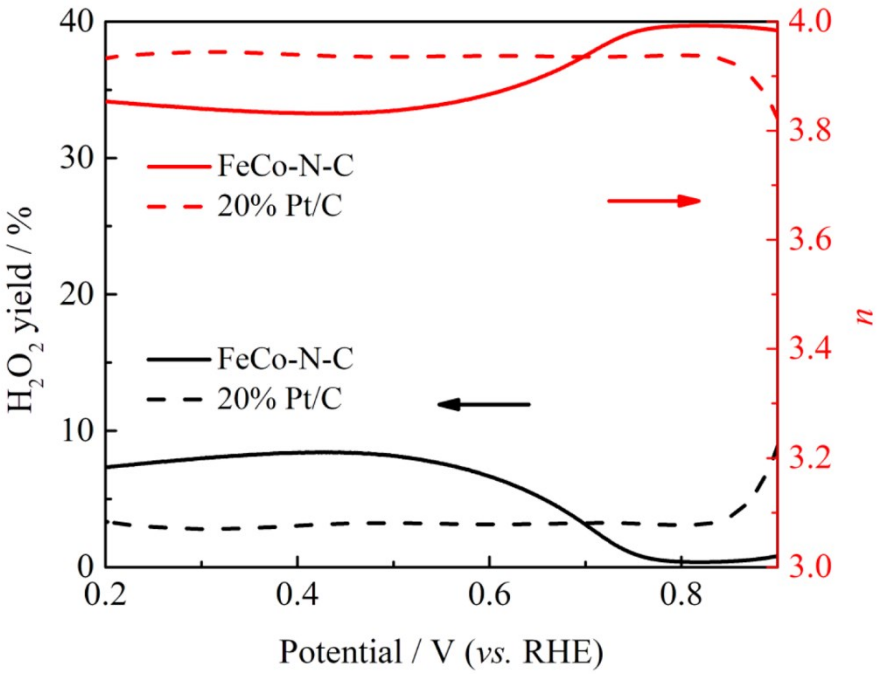

Fig. S13 Peroxide yields and the electron transfer number (*n*) for FeCo-N-C and 20% Pt/C.

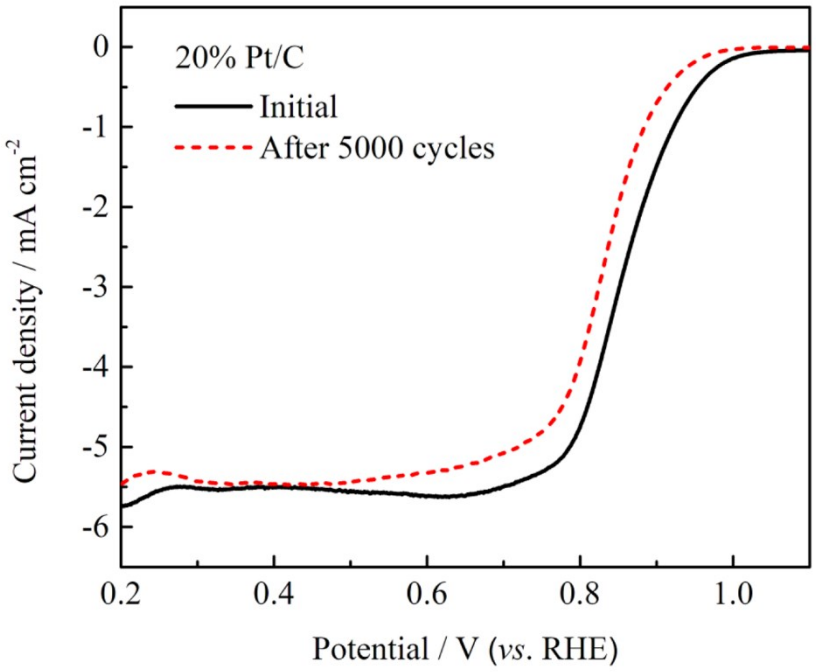

Fig. S14 ORR polarization curves of 20% Pt/C at 1600 rpm with a scan rate of 10 mV s^{-1} before and after 5000-cycle ORR ADT in 0.1 M KOH.

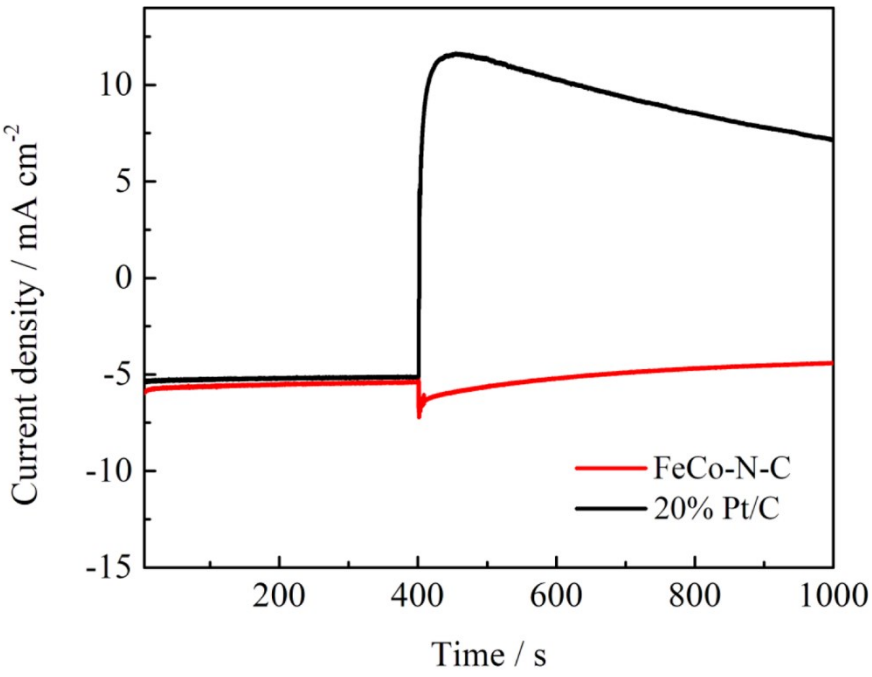

Fig. S15 Chronoamperometric response of FeCo-N-C and 20% Pt/C at 0.75 V under rotation speed of 1600 rpm after adding methanol in 0.1 M KOH.

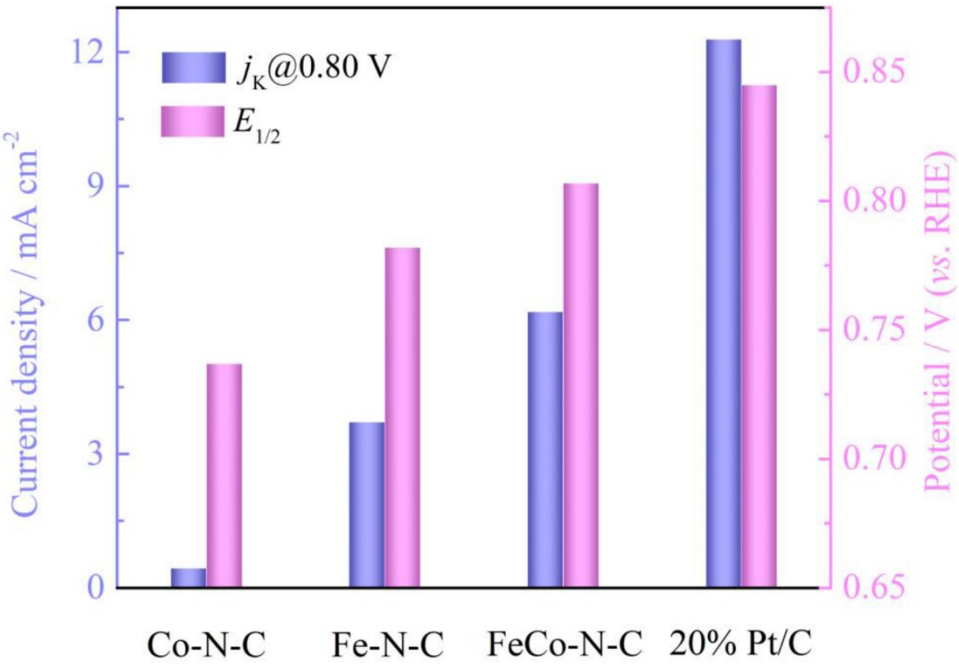

Fig. S16 The j_K at 0.8 V and $E_{1/2}$ for Co-N-C, Fe-N-C, FeCo-N-C and 20% Pt/C in 0.1 M $HClO_4$.

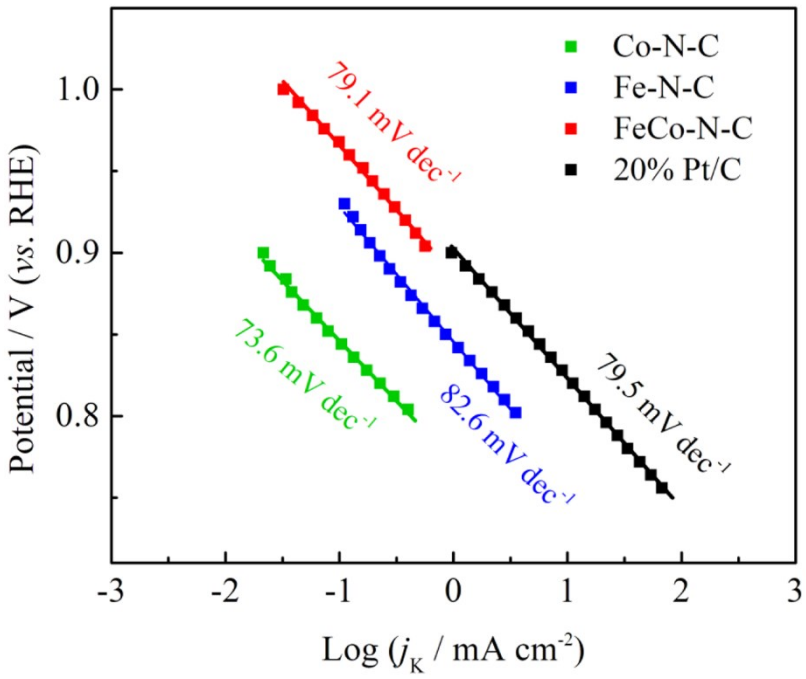

Fig. S17 Tafel plots for Co-N-C, Fe-N-C, FeCo-N-C and 20% Pt/C in 0.1 M $HClO_4$.

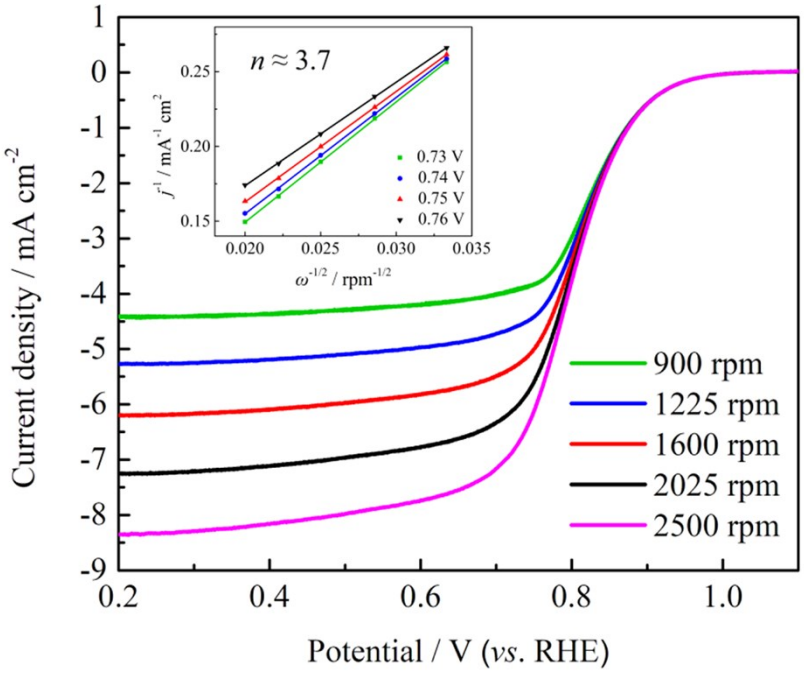

Fig. S18 ORR polarization curves at different rotating rates in 0.1 M $HClO_4$. Inset: the fitted K-L plots and electron transfer numbers.

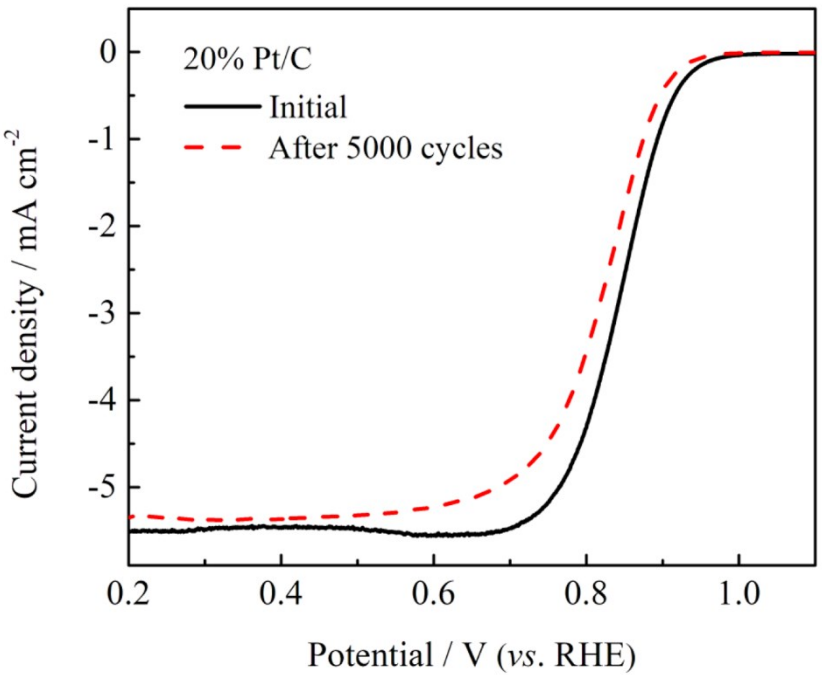

Fig. S19 ORR polarization curves of 20% Pt/C at 1600 rpm with a scan rate of 10 mV s^{-1} before and after 5000-cycle ORR ADT in 0.1 M $HClO_4$.

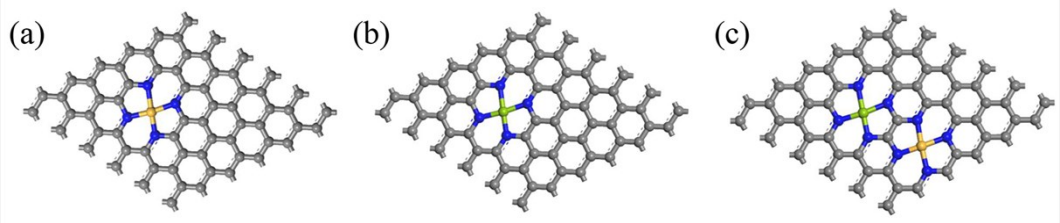

Fig. S20 Structure of (a) Co-N_4, (b) Fe-N_4, and (c) Fe-N_4&Co-N_4 sites where gray, blue, orange and green balls represent carbon, nitrogen, cobalt, and iron atoms, respectively.

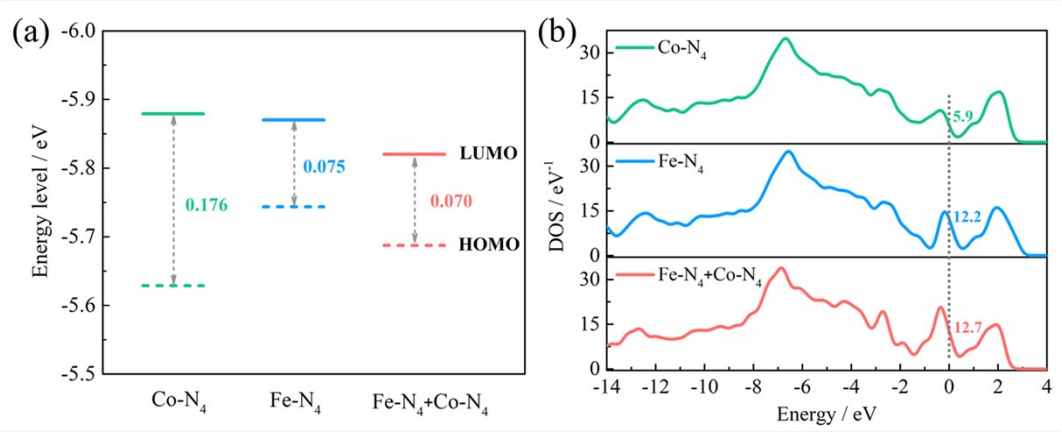

Fig. S21 (a) Energy levels of the HOMO and LUMO, along with the energy gap between them. (b) Density of state of $Co\text{-}N_4$, $Fe\text{-}N_4$, and $Fe\text{-}N_4$&$Co\text{-}N_4$.

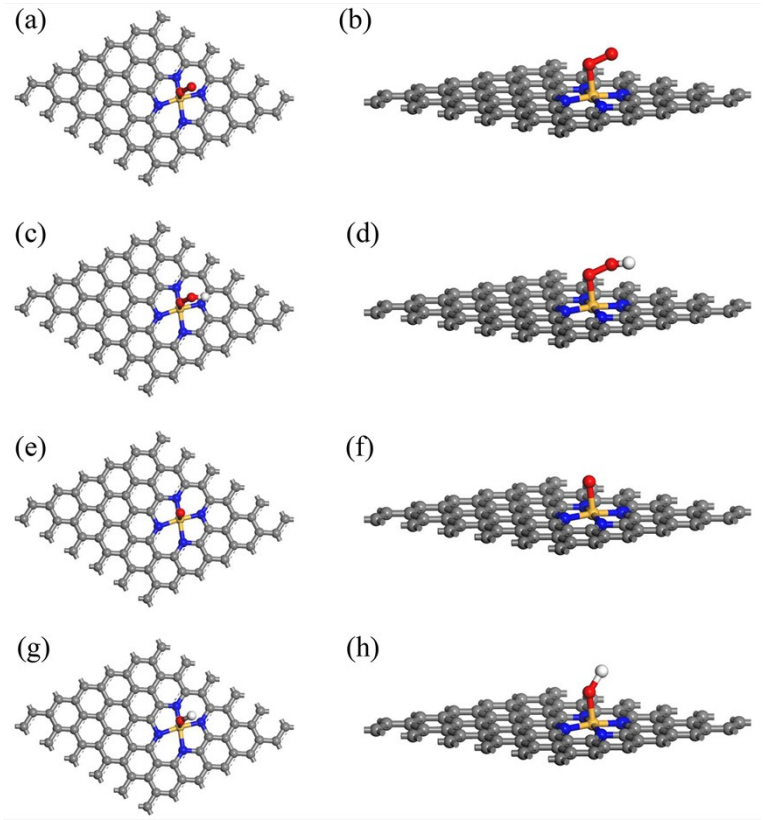

Fig. S22 (a, c, e, g) Top view and (b, d, f, h) side view of the adsorption configurations of the ORR intermediates on the surface of Co-N_4 site where gray, blue, orange, red, and white balls represent carbon, nitrogen, cobalt, oxygen, and hydrogen atoms, respectively.

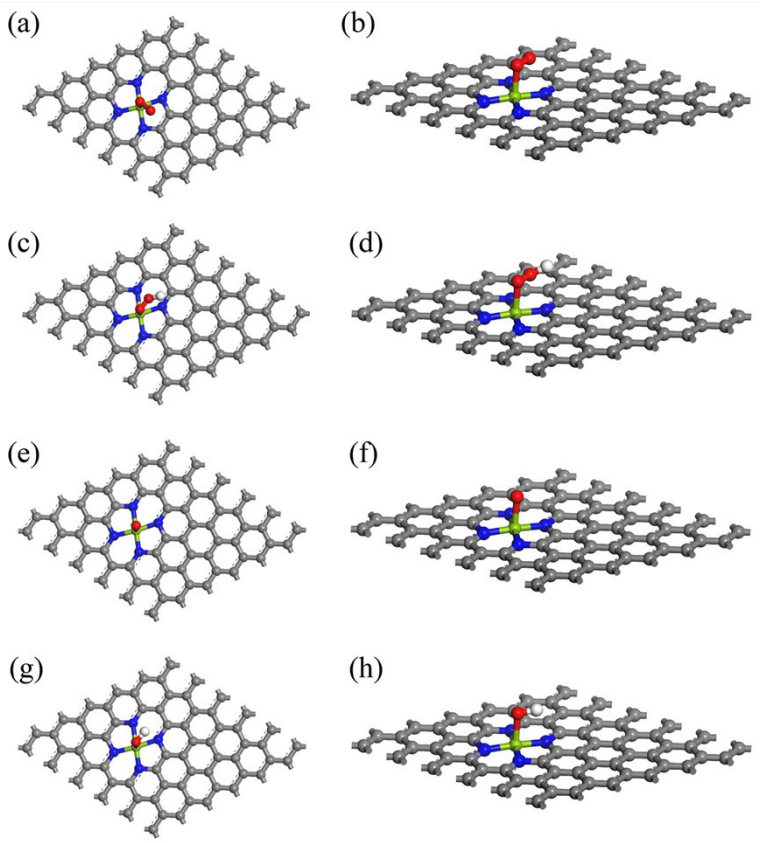

Fig. S23 (a, c, e, g) Top view and (b, d, f, h) side view of the adsorption configurations of the ORR intermediates on the surface of Fe-N_4 site where gray, blue, green, red, and white balls represent carbon, nitrogen, iron, oxygen, and hydrogen atoms, respectively.

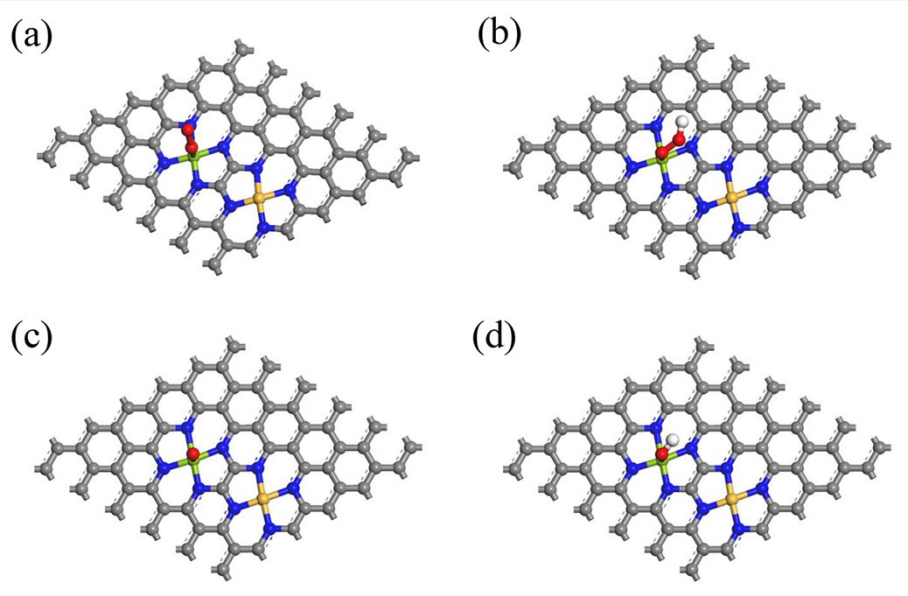

Fig. S24 Top view of the adsorption configurations of the ORR intermediates on the surface of Fe-N_4&Co-N_4 site where gray, blue, orange, green, red, and white balls represent carbon, nitrogen, cobalt, iron, oxygen, and hydrogen atoms, respectively.

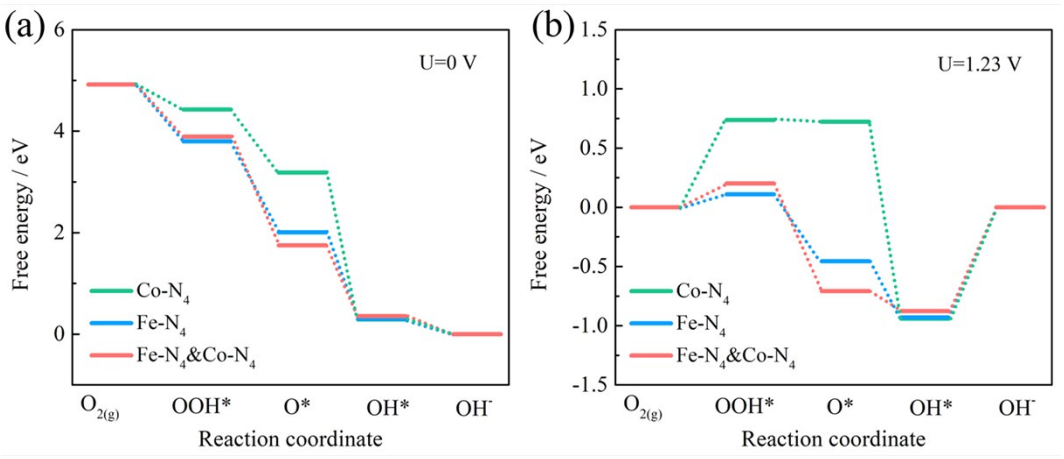

Fig. S25 Free energy diagram for the Co-N_4, Fe-N_4 and Fe-N_4&Co-N_4 systems during the ORR under alkaline condition at (a) U = 0 and (b) U = 1.23 V, respectively.

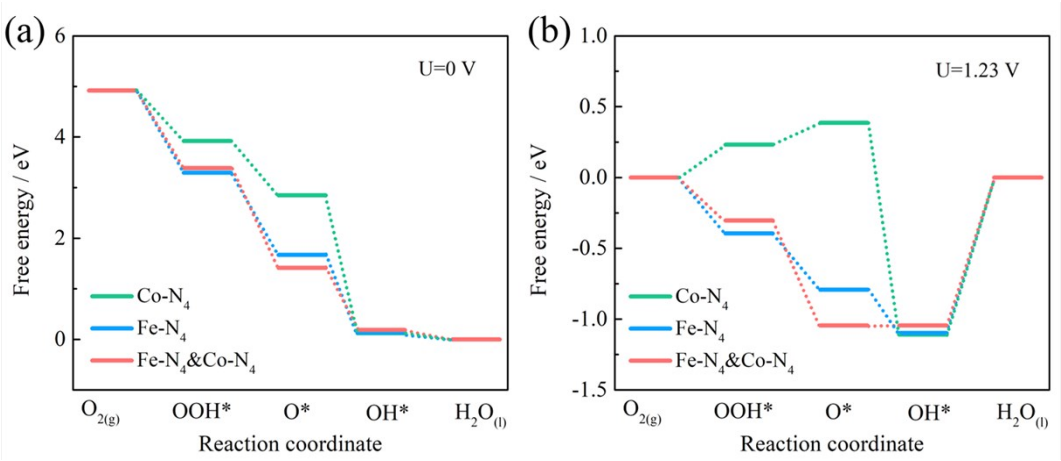

Fig. S26 Free energy diagram for the Co-N_4, Fe-N_4 and Fe-N_4&Co-N_4 systems during the ORR under acidic condition at (a) U = 0 and (b) U = 1.23 V, respectively.

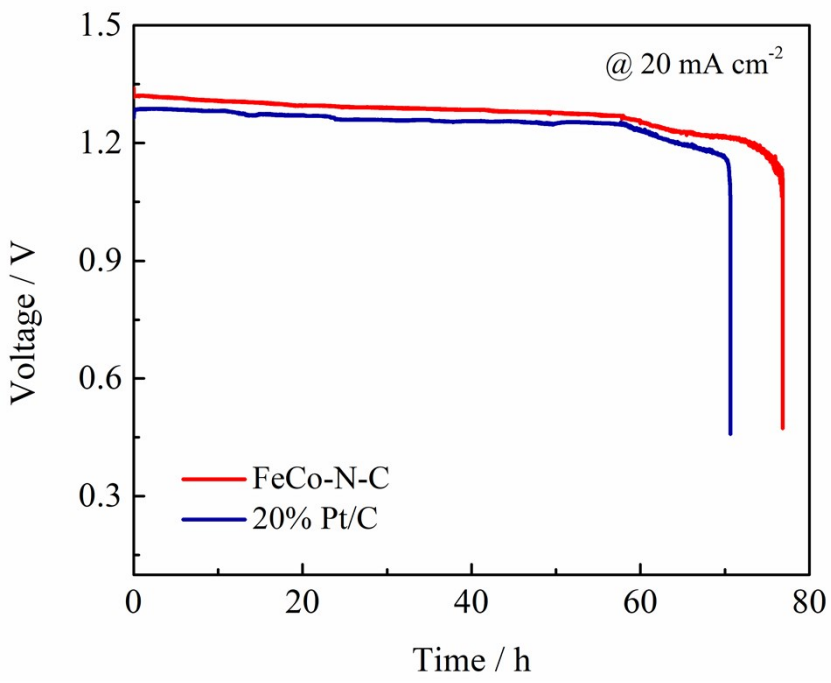

Fig. S27 Discharge curves of the liquid Zn-air batteries using FeCo-N-C and 20% Pt/C as air cathode at a current density of 20 mA cm^{-2}.

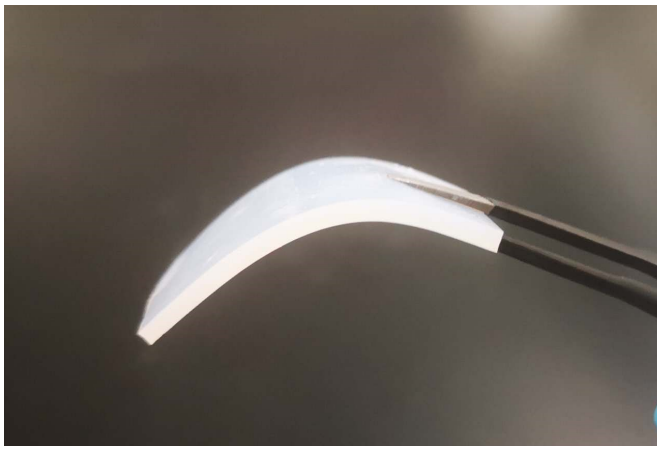

Fig. S28 A digital image of as-prepared flexible PVA gel film.

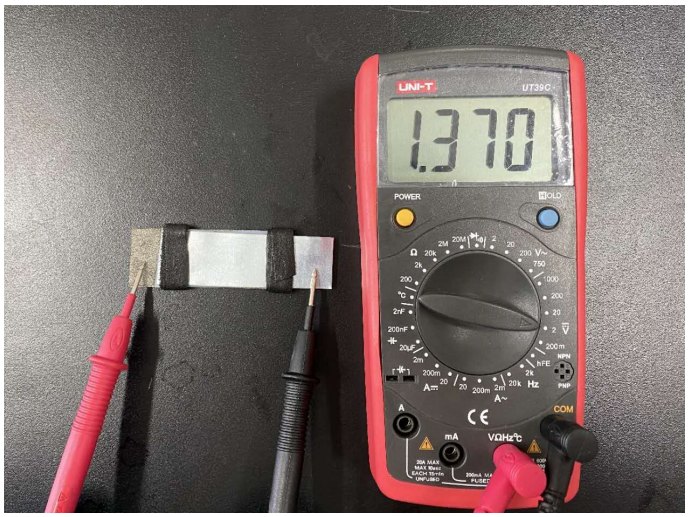

Fig. S29 A digital image of all-solid-state Zn-air battery exhibiting a minimum open-circuit voltage of ≈1.370 measured with a multimeter.

Table S1. Structural parameters extracted from the fitting EXAFS results at Fe K-edge (S_0^2=0.726) and Co K-edge (S_0^2=0.727).

sample	Scattering path	N	R(Å)	σ^2 (10^{-3}Å^2)	ΔE_0 (eV)	R factor
Fe foil	Fe-Fe	8	2.46	5.0	5.0	0.0058
	Fe-Fe	6	2.85	5.2	4.8	
FeCo-N-C	Fe-N	4.2	2.00	5.0	-1.3	0.0025
Co foil	Co-Co	12	2.49	6.0	7.3	0.0021
FeCo-N-C	Co-N	3.7	1.92	6.3	2.0	0.0097

S_0^2: amplitude reduction factor; N: coordination number; R: interatomic distance; σ^2: Debye-aller factor; ΔE_0: energy shift; R factor is used to value the goodness of the fitting.

Table S2. The content of C, N, O, Fe and Co of the prepared catalysts obtained from XPS.

	Atomic Concentration %					Mass Concentration %				
	C	N	O	Fe	Co	C	N	O	Fe	Co
Co-N-C	86.60	5.74	7.29	—	0.37	82.62	6.38	9.26	—	1.74
Fe-N-C	88.75	5.43	5.40	0.42	—	85.15	6.08	6.91	1.86	—
FeCo-N-C	86.17	6.68	6.69	0.12	0.34	81.99	7.41	8.48	0.54	1.57

Table S3. A comparison table of the ORR performance between this work and recently reported bimetal catalysts in alkaline and acidic media.

Materials	$E_{1/2}$ (V) (*vs.* RHE) in 0.1 M KOH	$E_{1/2}$ (V) (*vs.* RHE) in 0.1 M $HClO_4$	References
FeCo-N-C	0.904	0.807	This work
FeCo-IA/NC	0.88	—	J. Mater. Chem. A, 2020, 8, 4369
Fe-Cu-N/C	0.89	0.71	Nano Energy, 2017, 37, 187-194
FeCo-N-C-700	0.896	—	J. Mater. Chem. A, 2020, 8, 9355
Zn/CoN-C	0.861	0.796	Angew. Chem. Int. Ed., 2019, 58, 2622-2626
CuCo@NC	0.884	—	Adv. Energy Mater., 2017, 7, 1700193
CoPNi-N/C	0.81	0.70	Appl. Catal. B Environ., 2019, 240, 112-121
2D ZnCoFe/NC-850	0.831	—	J. Power Sources, 2019, 434, 226717
Fe, Mn-N/C	0.904	—	J. Mater. Chem. A, 2018, 6, 13254

FeCo-NC	0.855	0.63	Int. J. Hydrogen Energy, 2018, 43, 14701-14709
CoNi/BCF	0.80	—	Appl. Catal. B Environ., 2019, 240, 193-200

Table S4 Adsorption energies (eV) of ORR intermediates on Co-N_4, Fe-N_4, and Fe-N_4&Co-N_4 sites, respectively.

	$*O_2$	*OOH	*O	*OH
Co-N_4	-0.77	-1.35	-3.07	-2.89
Fe-N_4	-1.47	-1.97	-4.50	-3.08
Fe-N_4&Co-N_4	-1.29	-1.88	-4.24	-3.02

Table S5. The Bader charge (in e) for metal atoms in Co-N_4, Fe-N_4, and Fe-N_4&Co-N_4, structures, respectively.

Structure	Co	Fe
Co-N_4	0.454	——
Fe-N_4	——	0.502
Fe-N_4&Co-N_4	0.389	0.489

Table S6. A summary of the performance of liquid and all-solid-state Zn-air batteries with M-N-C catalysts.

Materials	liquid Zn-air batteries			all-solid-state Zn-air batteries	References
	Peak power density (mW cm^{-2})	specific capacity (mAh·g_{Zn}^{-1})	Energy density (Wh kg_{Zn}^{-1})	Peak power density (mW cm^{-2})	
FeCo-N-C	196.3	728.6	936.3	128.2	This work
CoNi/BCF	155.1	710.9	853.1	—	Appl. Catal. B Environ., 2019, 240, 193-200
FeCo-N-C-700	150	518	—	—	J. Mater. Chem. A, 2020, 8, 9355-9363
SilkNC/KB	91.2	614.7	727.6	32.3	Chem. Mater. 2019, 31, 1023-1029
NGM-Co	152	750	840	~28	Adv. Mater. 2017, 29, 1703185
FeCo-IA/NC	115.6	635.3	725.6	—	J. Mater. Chem. A, 2020, 8, 4369-4375
(Fe,Co)/CNT	260	774	870	—	Energy Environ. Sci., 2018, 11, 3375--3379

Fe@C-NG/NCNTs	101.3	682.6	764.5	—	J. Mater. Chem. A, 2018, 6, 516-526
3C-900	~97	727	819	—	J. Mater. Chem. A, 2018, 6, 3730-3737